Oscillatory free-induction decay

Axel Schenzle,* N. C. Wong, and Richard G. Brewer
IBM Research Laboratory, San Jose, California 95193
and Department of Applied Physics, Stanford University, Stanford, California 94305
(Received 19 September 1979)

Large-amplitude oscillations are predicted in the free-induction decay (FID) of atomic or spin two-level quantum systems that are coherently prepared by a resonant electromagnetic field in the form of a square amplitude pulse of duration T. The effect should be detectable in nuclear magnetic resonance (NMR) or in optical resonance experiments when the transition line shape is inhomogeneously broadened ($T_2^* \ll T_2$) and the applied field is intense enough that the pulse area $\chi T \geq 2\pi$, where χ is the Rabi frequency. Physically, the effect is due to Rabi oscillations which are generated in the preparative stage and are then reproduced because of atomic memory in the radiative period which follows. The atomic polarization derived from the Bloch equations assumes the form of an integral over the inhomogeneous line shape, and can be evaluated numerically for arbitrary linewidth σ or analytically when $\sigma \to \infty$. The characteristics of the oscillation are unusual since the oscillation frequency, which is of order χ, increases with time while the oscillation envelope vanishes identically for times $t \geq 2T$. Coherent emission is therefore confined to one pulse width T immediately following the pulse. Previous NMR and infrared FID experiments with small-area pulses ($\chi T \leq 4\pi$), interpreted erroneously in terms of an *edge echo* effect, support the oscillatory FID behavior described here. For the case $\chi T > 4\pi$, an experimental test would be even more decisive, as the oscillations are more pronounced.

I. INTRODUCTION

In this paper we predict a novel oscillatory behavior which appears in the free-induction-decay (FID) effect and should be observable in inhomogeneously broadened transitions, either in nuclear-magnetic-resonance (NMR) or in optical-resonance experiments. We assume a set of two-level quantum systems which are coherently prepared by a resonant driving field in the form of a square amplitude pulse of duration T. (See Fig. 1.) The transition line shape is dominated by inhomogeneous broadening so that the inhomogeneous dephasing time T_2^* and the dipole dephasing time T_2 satisfy the inequality

$$T_2 \gg T_2^* . \tag{1.1}$$

Following the pulse, FID occurs where the decay is smoothly varying for low field amplitudes. However, as the field intensity increases, we find that the decay exhibits a continuous train of large-amplitude oscillations (Figs. 2 and 3) which have not been discussed heretofore. Oscillations appear when the pulse area satisfies

$$\chi T \geq 2\pi , \tag{1.2}$$

and in first approximation, the oscillation frequency is the Rabi frequency χ. We also show that the FID signal is exactly zero for times $t \geq 2T$, as in Figs. 2 and 3. These and other characteristics are considered further in the theoretical analysis which follows.

Oscillatory FID, therefore, differs significantly from previous observations[1-8] of FID in the optical region. In the earlier optical studies, the sample is prepared under steady-state conditions by a cw laser beam, rather than by a pulse, and FID results when the transition frequency or the laser frequency is suddenly switched. The initial transient is dominated by the first-order FID.[2,7] which is a Gaussian $\exp[-(t/T_2^*)^2]$ that decays rapidly in a time T_2^*. The nonlinear FID survives the first-order component by displaying a long-lived exponential signal S which, apart from unimportant factors, is of the form[1,9]

$$S \sim (1/(\chi^2 T_1 T_2 + 1)^{1/2} - 1) \times \exp\{-t/T_2[1 + (\chi^2 T_1 T_2 + 1)^{1/2}]\} . \tag{1.3}$$

In this case, an increase in laser intensity only produces power broadening through the χ^2 term in the exponent, but no frequency shift and thus no oscillations. Of course, in the low-power limit ($\chi^2 T_1 T_2 \ll 1$), the dephasing time is $\frac{1}{2}T_2$, corresponding to preparation of a single homogeneous packet.

Oscillatory FID of this kind is not observed normally in NMR either. Because spin transitions

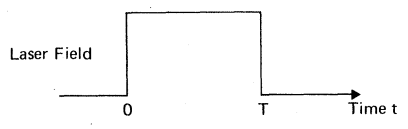

FIG. 1. Laser field vs time. The field is nonzero only in the interval $0 \leq t \leq T$.

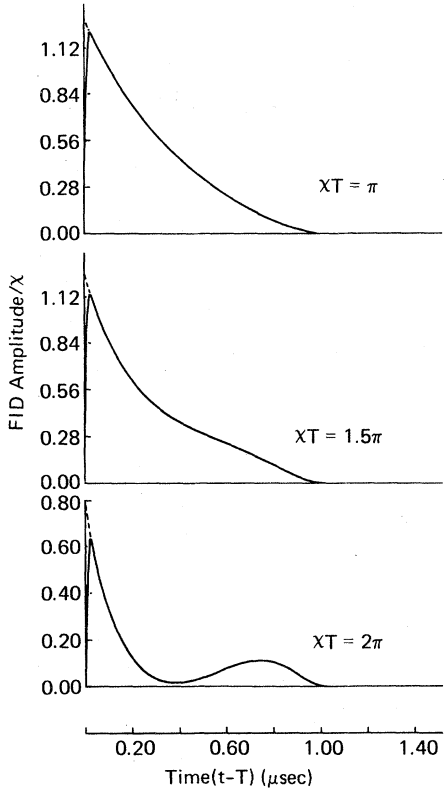

FIG. 2. Computer plots of free-induction-decay amplitude vs time as a function of laser pulse area χT. Solid curves: direct numerical integration of Eq. (2.15) for a Doppler-broadened line shape of finite width σ. The following parameters were assumed: $\sigma = 50\pi$ μsec^{-1}, $T = 1$ μsec, and $\gamma = 0$. Dashed curves: Bessel-function sum Eq. (3.37) where $\sigma \to \infty$.

often are homogeneously broadened, on-resonance pulse preparation can only yield FID signals which decay monotonically as $\exp(-t/T_2)$, while off-resonance preparation produces oscillations but they have a different origin.[10] Furthermore, the oscillations described here have nothing to do with quantum[11] or Raman beats[12] in coupled multilevel quantum systems or with NMR interferences in the FID of two or more independent two-level transitions.

However, Bloom[13] reported observations of NMR interference effects in FID for the case when the static magnetic field is highly inhomogeneous and the pulse area $\chi T \simeq 4\pi$ is relatively small. We believe that these interferences, which Bloom gave the name "edge echoes," are not an echo phenomenon, but rather are an example of oscillatory FID. This paper clarifies the subject by providing the first detailed theoretical treatment of oscillatory FID.

II. THEORETICAL MODEL

A. Basic equations

We shall adopt a model and the mathematical language commonly used in quantum optics,[14,15] namely, an atomic two-level quantum system which interacts for the period T with a resonant laser field

$$E_x(z,t) = E_0 \cos(\Omega t - kz). \tag{2.1}$$

The polarization and propagation directions are x and z, respectively. The upper quantum state is $|2\rangle$ and the lower $|1\rangle$. We assume that the field is turned on at $t = 0$ and off at $t = T$. Equivalently, we could have also assumed a laser frequency-switching[3,6] pulse as the solutions are virtually identical.

For times $t > T$ following the pulse, the FID field

$$E_{12}(z,t) = \tilde{E}_{12}(z,t) e^{i(\Omega t - kz)} + \text{c.c.} \tag{2.2}$$

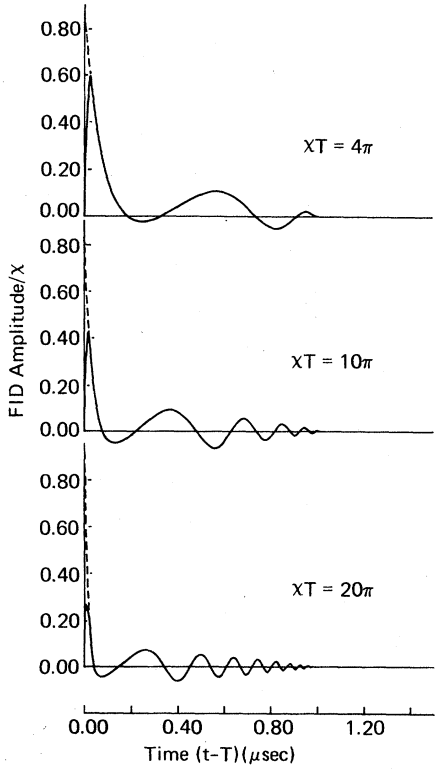

FIG. 3. Computer plots of free-induction-decay amplitude vs time as a function of laser pulse area χT. Solid curves: direct numerical integration of Eq. (2.15) for a Doppler-broadened line shape of finite width σ. The following parameters were assumed: $\sigma = 50\pi$ μsec^{-1}, $T = 1$ μsec, and $\gamma = 0$. Dashed curves: Bessel-function sum Eq. (3.37) where $\sigma \to \infty$.

satisfies Maxwell's wave equation

$$\frac{\partial \tilde{E}_{12}}{\partial z} = -2\pi i k N \mu_{12} \langle \tilde{\rho}_{12} \rangle \tag{2.3}$$

for an optically thin sample. Here N is the atomic number density, μ_{12} is the transition matrix element, and the tilde denotes the slowly varying part. Hence the problem reduces to one of calculating the polarization

$$\langle \tilde{p}(t) \rangle = N \,\mathrm{Tr} \langle \mu \tilde{\rho}(t) \rangle , \tag{2.4}$$

where the off-diagonal density-matrix element $\tilde{\rho}_{12}$ is to be averaged (denoted by a bracket) over the inhomogeneous Doppler line shape. We therefore seek solutions of the Bloch equations

$$\begin{aligned} &\dot{u} + \Delta v + u/T_2 = 0 , \\ &\dot{v} - \Delta u - \chi w + v/T_2 = 0 , \\ &\dot{w} + \chi v + (w - w^0)/T_1 = 0 , \end{aligned} \tag{2.5}$$

where

$$u = \tilde{\rho}_{12} + \tilde{\rho}_{21} , \quad v = i(\tilde{\rho}_{21} - \tilde{\rho}_{12}), \quad w = \rho_{22} - \rho_{11} . \tag{2.6}$$

The tuning parameter Δ, the Rabi frequency χ, and the eigenenergies E_i are given by

$$\Delta = -\Omega + k v_z + \omega_{21}, \quad \chi = \mu_{12} E_0/\hbar, \quad E_i = \hbar \omega_i \quad (i = 1, 2). \tag{2.7}$$

where kv_z is the Doppler shift and $\omega_{21} \equiv \omega_2 - \omega_1$.

To avoid unnecessary complications, we assume that (i) the population and dipole dephasing rates are equal, (ii) the Rabi frequency is much larger than the dipole dephasing rate, and (iii) the laser frequency is tuned to the transition line center; i.e.,

$$\gamma \equiv 1/T_1 = 1/T_2 , \tag{2.8}$$

$$\chi^2 \gg \gamma^2 , \tag{2.9}$$

$$\Omega = \omega_{21} . \tag{2.10}$$

With the approximation (2.8) and the initial conditions $v(t=0) = u(0) = 0$ and $w(0) = w^0$, the solutions of (2.5) are

$$\begin{aligned} v(t) &= \frac{\chi w(0) e^{-\gamma t}}{\chi^2 + \Delta^2 + \gamma^2} (-\gamma \cos\beta t + \beta \sin\beta t + \gamma e^{\gamma t}) , \\ u(t) &= \frac{\Delta \chi w(0) e^{-\gamma t}}{\chi^2 + \Delta^2 + \gamma^2} \left(\frac{\gamma \sin\beta t}{\beta} + \cos\beta t - e^{\gamma t} \right), \end{aligned} \tag{2.11}$$

where

$$\beta = (\Delta^2 + \chi^2)^{1/2} .$$

Equations (2.11) will be required when damping is to be included, but for the present purpose, we invoke (2.9) and obtain the relevant solutions for pulse preparation at time $t = T$,

$$\begin{aligned} v(T) &= \chi w(0) e^{-\gamma T} (\sin\beta T)/\beta , \\ u(T) &= [\Delta \chi w(0)/\beta^2](e^{-\gamma T} \cos\beta T - 1) . \end{aligned} \tag{2.12}$$

In the next stage $t > T$, $\chi = 0$, and the FID solutions of (2.5) apply,

$$\begin{aligned} u(t) &= [u(T) \cos\Delta(t - T) - v(T) \sin\Delta(t - T)] e^{-\gamma(t-T)} \\ v(t) &= [u(T) \sin\Delta(t - T) + v(T) \cos\Delta(t - T)] e^{-\gamma(t-T)} . \end{aligned} \tag{2.13}$$

Inserting Eq. (2.12) into Eq. (2.13), we obtain the desired result for $t > T$,

$$\begin{aligned} v(t) = \chi w(0) e^{-\gamma t} [(\Delta/\beta^2)(\cos\beta T - e^{\gamma T}) \sin\Delta(t - T) \\ + (\sin\beta T/\beta) \cos\Delta(t - T)] . \end{aligned} \tag{2.14}$$

The dispersive term $u(t)$ is not needed, as it vanishes with Doppler integration owing to its odd-order dependence in Δ and assumption (2.10).

The FID signal (2.2) therefore involves the Doppler integral I, where

$$N \langle \tilde{\rho}_{12}(t) \rangle = \tfrac{1}{2} i \int_{-\infty}^{\infty} g(\Delta) v(t) d\Delta \equiv \tfrac{1}{2} i I(t) , \tag{2.15}$$

the inhomogeneous line-shape function

$$g(\Delta) = (N/\sqrt{\pi}\sigma) e^{-(\Delta/\sigma)^2} , \tag{2.16}$$

and the Doppler width is σ.

The major challenge of this paper is the evaluation of the integral (2.15). Analytic results are not anticipated because of the Gaussian term in the integrand, and furthermore, the square root $\beta = (\Delta^2 + \chi^2)^{1/2}$ can introduce a troublesome branch cut in the complex plane. In Sec. II B, (2.15) is evaluated by direct numerical integration and allows a preliminary understanding of the nature of oscillatory FID. The remaining sections uncover analytic results in the limit of an infinite Doppler linewidth ($\sigma \to \infty$), and give a more detailed and complete description of the phenomena involved. In Sec. III A, certain limiting cases are derived by means of a Laplace-transform method. In Sec. III B, a general analytic expression of compact form is found by transforming the integral (2.15) to a differential equation.

B. Numerical results

Figures 2 and 3 are computer plots of the normalized FID amplitude E_{12}/χ, as a function of time $(t - T)$ and for different pulse areas χT. The solid curves result from direct numerical integration of (2.15), while the overlayed dashed curves are analytic results of Sec. III B and are discussed below.

The following parameter values were assumed: $\sigma = 50\pi$ μsec^{-1}, $T = 1$ μsec, and $\gamma = 0$, and hence the desired inequalities $\sigma > \chi > 1/T > \gamma$ were maintained.

Consideration is given in Sec. III A to the case $\gamma \neq 0$. Obviously, other time scales apply to these curves when an appropriate change is made in the time-frequency units. We find that about $100\sigma T$ integration points are needed to attain the required accuracy for the Doppler integration.

The first characteristic to notice in Figs. 2 and 3 is the initial fast rise beginning at $t = T$ which appears on all solid curves. This is the first-order free-induction-decay effect which has been observed[7] and analyzed theoretically[2,7] for the case of steady-state preparation. For both pulse and steady-state preparation, the rise time is given by $T_2^* \equiv 2/\sigma$. The Doppler line shape, being of finite width, allows the FID signal to rise smoothly from its initial value at $t = T$. In the limit of infinite Doppler width, the signal is discontinuous at $t = T$, as found in such previous FID derivations[1,2,9] as Eq. (1.3).

For times $(t - T) > T_2^*$, the decay is more slowly varying and exhibits oscillations which are clearly evident in Figs. 2 and 3 for pulse areas $\chi T \geq 2\pi$. Note in particular the curve for $\chi T = 4\pi$, as it closely resembles Bloom's NMR free decay[13] (his Fig. 4, where $\chi T \cong 4\pi$) in shape, the number of oscillations, and its vanishing at $t = 2T$. We believe this observation strongly supports our calculation. However, the term "edge echo" coined by Bloom is inappropriate as the effect is not an echo phenomenon.

As the pulse area increases further, the number of oscillations increases, the number of periods being given by $\sim\chi T/2\pi$. Thus, for $\chi T = 10\pi$, there are five periods, where the last wiggle, being of small amplitude, is better seen on an expanded scale. These curves and the analysis of Sec. III show that in each case the last wiggle always approaches the time axis as $(2T - t)^2$ and from the positive direction as $t \to 2T$.

Another feature is that the oscillation frequency, while of order χ, is not constant but increases steadily with time. The envelope function of these oscillations obeys approximately a linear time dependence such that the amplitude vanishes precisely at time $t = 2T$. This remarkable behavior is an exact and general result which can be demonstrated by very general theoretical arguments and will be presented elsewhere.[16] An earlier optical FID measurement,[1] where $\chi T = 1.5\pi$, corroborates this point and otherwise resembles the $\chi T = 1.5\pi$ curve of Fig. 2.

Physical interpretation. As a first approximation, we can say that during the preparative stage the driving field creates Rabi sidebands and thus new frequency components which would be observed in a spectrum of the sample. Following the pulse, the polarization retains memory of its preparation and produces a time-dependent signal which is the Fourier transform of this spectrum, and hence oscillations will appear at the Rabi frequency. Of course, this picture neglects the mutual interference of packets distributed throughout the inhomogeneous line shape.

We can summarize this section, perhaps in an oversimplified manner, by pointing out that there are three parameters (σ, χ, and T) which characterize the temporal response of the atomic sample. The Doppler width σ gives rise to the initial rapid first-order FID, the Rabi frequency χ determines the frequency of oscillation, and the pulse width T establishes when the free-induction signal vanishes.

III. ANALYTIC RESULTS

A. Laplace-transform method

1. Case $\gamma = 0$

We now evaluate the Doppler integral $I(t)$ defined in (2.15) using (2.14) for $v(t)$ in the case $\gamma = 0$. We apply the Laplace-transform technique[17,18] because it yields the characteristic behavior for certain limiting cases very quickly. The case $\gamma \neq 0$ will be treated below as well. In the limit of infinite Doppler width ($\sigma \to \infty$), $\exp[-(\Delta/\sigma)^2] \to 1$ while the spectral density N/σ is constant, and

$$I(t) = \chi w(0) g(0) \left(\int_{-\infty}^{\infty} \frac{\sin\beta T}{\beta} \cos\Delta(t - T) d\Delta + \int_{-\infty}^{\infty} \frac{\Delta}{\beta^2} \cos\beta T \sin\Delta(t - T) d\Delta - \int_{-\infty}^{\infty} \frac{\Delta}{\beta^2} \sin\Delta(t - T) d\Delta \right), \quad t > T. \tag{3.1}$$

We identify the three integrals in the order given by

$$I(t) = \chi w(0) g(0) [F_1(t) + F_2(t) + F_3(t)], \tag{3.2}$$

and perform the Laplace transform

$$F(z) = \int_0^{\infty} F(T) e^{-zT} dT \equiv \mathcal{L} F(T) \tag{3.3}$$

in the variables z and T with the quantity $t - T$ held fixed. This operation yields

$$F_1(z) = [\pi/(z^2 + \chi^2)^{1/2}] \exp[-(z^2 + \chi^2)^{1/2}(t - T)], \tag{3.4}$$

$$F_2(z) = (\pi/z)\{e^{-\chi(t-T)} - \exp[-(z^2 + \chi^2)^{1/2}(t - T)]\}, \tag{3.5}$$

$$F_3(z) = -(\pi/z) e^{-\chi(t-T)}. \tag{3.6}$$

Note that two of the terms cancel in the sum

$$I(z) = \chi w(0) g(0) [F_1(z) + F_2(z) + F_3(z)] = -\pi\chi w(0) g(0) G(z)/z, \tag{3.7}$$

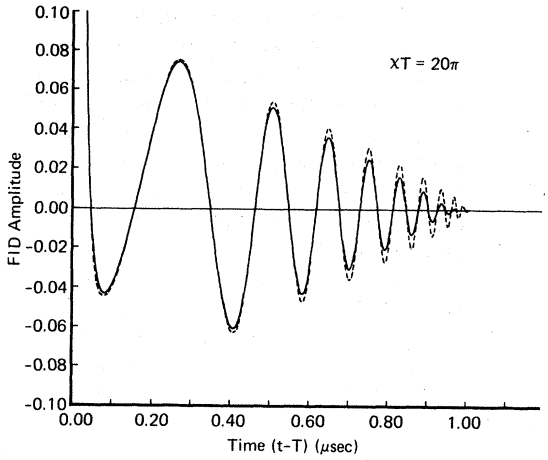

FIG. 4. Computer plot of FID vs time for a pulse area $\chi T = 20\pi$. Solid curve: direct numerical integration of Eq. (2.15) where $\sigma = 50\pi$ μsec^{-1}, $\chi = 20\pi$ μsec^{-1}, and $T = 1$ μsec. Dashed curve: Bessel-function sum Eq. (3.37) where the number of terms used in the series is $m = 90$.

where

$$G(z) = [1 - z/(z^2+\chi^2)^{1/2}]\exp[-(z^2+\chi^2)^{1/2}(t-T)]. \quad (3.8)$$

Recognizing that the inverse Laplace transform of (3.7) is given by

$$\mathcal{L}^{-1}G(z)/z = \int_0^T G(T')dT', \quad (3.9)$$

we need

$$\mathcal{L}^{-1}G(z) = G(T) = \begin{cases} 0, & 0 < T < t - T, \quad (3.10a) \\ \chi\left(\dfrac{T-(t-T)}{T+(t-T)}\right)^{1/2} J_1(\chi[T^2-(t-T)^2]^{1/2}), & T > t - T, \quad (3.10b) \end{cases}$$

where this transformation is tabulated.[19] Combining (3.7)–(3.10), we obtain for the integrals in (3.1) the compact form

$$I(t) = \begin{cases} 0, & t > 2T, \quad (3.11a) \\ -\pi w(0)g(0)\chi^2 \displaystyle\int_{t-T}^{T} \left(\frac{s-(t-T)}{s+(t-T)}\right)^{1/2} J_1(\chi[s^2-(t-T)^2]^{1/2})ds, & T < t < 2T. \quad (3.11b) \end{cases}$$

Note the interesting result (3.11a), which states that, for times $t > 2T$, coherent emission is identically zero. Stated otherwise, when a two-level quantum system is coherently prepared in the interval $0 < t < T$, it radiates coherently only in the interval $T < t < 2T$. We have shown elsewhere[16] that this result is true under very general conditions, a theoretical result which apparently has gone unnoticed in NMR and quantum optics.

Limiting cases. In order to see how the solution (3.11b) connects to the solutions for $t < T$ and $t > 2T$, we consider the following limiting cases:

$t \to T$: In this limit, (3.11b) is given by

$$I(t \to T) = \pi w(0)g(0)\chi[J_0(\chi T) - 1]. \quad (3.12)$$

Since $J_0(\chi T)$ is the transient nutation amplitude at the end of the pulse, we recognize that the -1 term signifies a discontinuity at $t = T$ which we attribute to the first-order FID for the case of infinite Doppler width. Additional attention is given below to first-order FID when the Doppler width is finite.

$t \to 2T$: In this regime, since the argument α of the Bessel function[20] $J_1(\alpha)$ remains small throughout the range of integration,

$$J_1(\alpha) \simeq \tfrac{1}{2}\alpha,$$

and

$$I(t \to 2T) = -\tfrac{1}{4}\pi w(0)g(0)\chi^3(2T-t)^2. \quad (3.13)$$

Because $w(0) = -1$, the FID signal approaches a zero value from the positive direction with a quadratic dependence in the time difference $2T - t$, independent of χT. Thus $I(t)$ and its first derivative are continuous at $t = 2T$ and exhibit no unusual characteristics such as an edge echo. Note that the numerical results of Sec. III B are therefore verified. In this connection, one should compare Bloom's[13] Fig. 4 for the case of a single pulse (which resembles our Fig. 3 for $\chi T = 4\pi$) and his Fig. 5 for the case of a closely spaced multiple-pulse train which produces a sharp interference near $t = 2T$. The multiple-pulse train is an entirely different situation from the single-pulse calculations discussed in this paper.

First-order FID. To investigate the first-order FID, also note that the only term in (3.1) which possesses a singularity at $t = T$ is $F_3(t)$. For the case of finite σ, we write

$$F_3'(t) = -\chi w(0)\int_{-\infty}^{\infty} g(\Delta)(\Delta/\beta^2)\sin\Delta(t-T)d\Delta. \quad (3.14)$$

For a Lorentzian inhomogeneous line shape

$$g(\Delta) = N(\sigma/\pi)1/(\Delta^2+\sigma^2) \quad (3.15)$$

instead of the Gaussian (2.16), we obtain an analytic expression in terms of elementary functions

$$F_3'(t) = -N[\chi w(0)\sigma/(\sigma^2-\chi^2)](e^{-\chi(t-T)} - e^{-\sigma(t-T)})$$
$$\simeq \pi\chi |w(0)| g(0) e^{-\chi(t-T)}(1 - e^{-\sigma(t-T)}), \quad (3.16)$$

where the second line applies when $\sigma \gg \chi$. Thus immediately following the end of the pulse the FID signal rises rapidly but smoothly in a time $1/\sigma \simeq T_2^*$, reaches a maximum at $(t-T)_{\max} = 1/\sigma \ln(\sigma/\chi)$, and then decays in a time $1/\chi$ prior to going into oscillation. The initial fast rise in the first-order FID[2,7] [which corresponds to the discontinuity at $t=T$ in (3.12) and (1.3) when $\sigma \to \infty$] and is readily seen in all of the numerical results of Figs. 2 and 3, where a Gaussian line shape of finite width σ is utilized.

$$I(t) = \begin{cases} 0, & t > 2T, \\ -\pi w(0) g(0) \chi^2 e^{-\gamma(t-T)} \int_{t-T}^{T} \left(\frac{s-(t-T)}{s+(t-T)}\right)^{1/2} J_1(\chi[s^2-(t-T)^2]^{1/2}) e^{-\gamma s}\, ds, & T < t < 2T. \end{cases} \quad (3.17)$$

Apart from damping factors, (3.17) maintains the same form as (3.11).

Limiting cases: *infinite pulse width* ($T \to \infty$). As the pulse width T increases, the solutions must approach the case of steady-state preparation.[1,2,7,9] This limit can be tested by using (3.17), in contrast to (3.11), because damping is needed to restore the population during continuous excitation. The integral (3.17) can be written as

$$\tau \int_1^{\infty} \left(\frac{y-1}{y+1}\right)^{1/2} J_1(\chi\tau(y^2-1)^{1/2}) e^{-\gamma y\tau}\, dy \quad (3.18)$$

and becomes analytic[21] as $T \to \infty$, where $\tau \equiv t - T$ remains finite and $y \equiv s/\tau$. The result is

$$I(t) = \pi w(0) g(0) \chi \left(\frac{1}{[(\chi/\gamma)^2+1]^{1/2}} - 1\right)$$
$$\times \exp(-\gamma\{1 + [(\chi/\gamma)^2+1]^{1/2}\}(t-T)), \quad (3.19)$$

which we see agrees with such earlier steady-state derivations as Eq. (1.3).[1,2,7,9]

$t \to T$: Equation (3.17) reduces in this instance to

$$I(t \to T) \simeq \pi w(0) g(0) \chi [J_0(\chi T) - 1] e^{-\gamma T}, \quad (3.20)$$

where for simplicity we have assumed that $\gamma \to 0$. As expected, (3.20) agrees with (3.12).

$t \to 2T$: In this regime, (3.17) becomes

$$I(t \to 2T) = -\tfrac{1}{4}\pi w(0) g(0) \chi^3 e^{-\gamma T}(2T-t)^2, \quad (3.21)$$

and corresponds to the no-damping case (3.13).

B. Differential-equation method

In this section, we again evaluate the Doppler integral expression $I(t)$ given in (3.1) assuming $\sigma \to \infty$ and $\gamma = 0$. The derivation is more lengthy than the Laplace-transform method, but it is also more instructive and reduces to a compact analytical form which is exact. For this purpose, the integral form of $I(t)$ is transformed by differentiation with respect to the variable T and yields the second-order differential equation

$$\frac{d^2I}{dT^2} - \chi^2 I = \left\langle \frac{2\chi^3}{\beta} \sin\beta T \cos\Delta(t-T) - \Delta\chi \sin\Delta(t-T) \right\rangle, \quad (3.22)$$

where the brackets denote a Doppler average and we have set $w(0) = -1$ throughout. The observation time t is treated as a constant.

We now show that

$$\frac{d^2I}{dT^2} - \chi^2 I = 0, \quad t > 2T, \quad (3.23a)$$

$$\frac{d^2I}{dT^2} - \chi^2 I = 2\pi g(0)\chi^3 J_0(\chi[t(2T-t)]^{1/2}), \quad T < t < 2T. \quad (3.23b)$$

Equation (3.23a) follows when a Lorentzian inhomogeneous line shape (3.15)

$$g(\Delta) = g(0)\sigma^2/(\Delta^2+\sigma^2) \quad (3.24)$$

is substituted for the Gaussian (2.16), as then the integrals[21] in (3.22) are analytic and vanish in the limit $\sigma \to \infty$. Thus we have

$$\left\langle \frac{2\chi^3}{\beta} \sin\beta T \cos\Delta(t-T) \right\rangle$$
$$= 2\pi g(0)\chi^3 \frac{\sigma e^{-\sigma(t-T)}}{(\sigma^2-\chi^2)^{1/2}} \sinh(\sigma^2-\chi^2)^{1/2} T, \quad t > 2T,$$
$$\to 0 \text{ as } \sigma \to \infty, \quad (3.25)$$

and

$$\langle -\Delta\chi \sin\Delta(t-T)\rangle = -\pi g(0)\chi\sigma^2 e^{-\sigma(t-T)}, \quad t > T,$$
$$\to 0 \text{ as } \sigma \to \infty, \quad (3.26)$$

where the initial conditions are

$$I(T=0) = 0,$$
$$\frac{dI(T=0)}{dT} = \langle -\chi \cos\Delta t\rangle = -\pi g(0)\chi\sigma e^{-\sigma t},$$
$$\to 0 \text{ as } \sigma \to \infty \text{ for } t > 0. \quad (3.27)$$

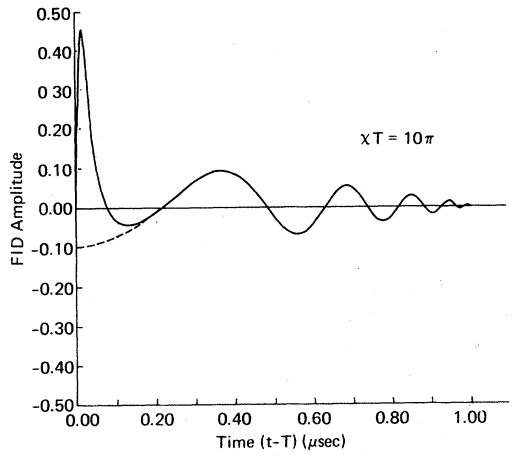

FIG. 5. Computer plot of FID vs time for a pulse area $\chi T = 10\pi$. Solid curve: direct numerical integration of Eq. (2.15) where $\sigma = 50\pi\ \mu\text{sec}^{-1}$, $\chi = 10\pi\ \mu\text{sec}^{-1}$, and $T = 1\ \mu\text{sec}$. Dashed curve: asymptotic function Eq. (3.39).

Thus (3.23a) is derived. On the other hand, (3.23b) follows from (3.26) and

$$\left\langle \frac{2\chi^3}{\beta} \sin\beta T \cos\Delta(t-T) \right\rangle = 2\pi g(0)\chi^3 J_0(\chi[t(2T-t)]^{1/2}), \quad T < t < 2T, \tag{3.28}$$

where $g(0)$ has been factored outside the integral to facilitate its evaluation.

From (3.23a) and the initial conditions (3.27), we obtain the same result as (3.11a),

$$I(t) = 0, \quad t > 2T. \tag{3.29}$$

Therefore, the FID signal lasts as long as the pulse width itself and vanishes for $t > 2T$.

Notice that the integrals (3.25) and (3.26) decay rapidly, as in first-order FID, because of the $e^{-\sigma(t-T)}$ factor. In contrast to first-order FID at the beginning of the pulse (Sec. III A), its amplitude is extremely small and is not evident in the numerical results of Figs. 2 and 3, where a finite Doppler width is assumed. Clearly the use of a Lorentzian line shape in place of a Gaussian does not change these arguments as $\sigma \to \infty$.

We now attempt to find the general solution of (3.23b)

$$I(\chi, t, T) = I_H(T) + I_p(T), \quad T < t < 2T, \tag{3.30}$$

where the homogeneous solution is of the form

$$I_H(T) = Ae^{\chi T} + Be^{-\chi T}, \tag{3.31}$$

and a particular solution, obtained by using the method of variation of parameters,[22] is

$$I_p(T) = \pi g(0)\chi^2 \left(\int_0^T e^{\chi(T-T')} J_0(\chi[t(2T'-t)]^{1/2}) dT' - \int_0^T e^{-\chi(T-T')} J_0(\chi[t(2T'-t)]^{1/2}) dT' \right). \tag{3.32}$$

Equation (3.32) can be written as

$$I_P(T) = 2\pi \frac{g(0)}{t} \int_0^z \sinh\left(\frac{z^2 - z'^2}{2\chi t}\right) z' J_0(z') dz', \tag{3.33}$$

where

$$z = \chi[t(2T-t)]^{1/2}.$$

In the Appendix, we show that (3.33) reduces simply to a sum of even-order Bessel functions

$$I_P(T) = 2\pi g(0)\chi \sum_{m=1}^{\infty} \left(\frac{z}{\chi t}\right)^{2m} J_{2m}(z). \tag{3.34}$$

Equation (3.34) and its derivative

$$\frac{dI_P}{dT} = 2\pi g(0)\chi \sum_{m=1}^{\infty} \left(\frac{z}{\chi t}\right)^{2m} J_{2m-1}(z), \tag{3.35}$$

yield the initial conditions

$$I_P(0) = \frac{dI_P(0)}{dT} = 0. \tag{3.36}$$

When (3.36) and (3.27) are combined, it follows that $I_H(T) \equiv 0$ and the solution (3.30) is

$$I(\chi, t, T) = I_P(T) = 2\pi g(0)\chi \sum_{m=1}^{\infty} \left(\frac{\alpha}{r}\right)^{2m} J_{2m}(\alpha\chi T), \tag{3.37}$$

where

$$r \equiv t/T \quad (2 > r > 1), \quad \alpha \equiv [r(2-r)]^{1/2} \quad (0 < \alpha < 1).$$

Returning to the FID computer plots of Figs. 2 and 3, we see that Eq. (3.37) (dashed curve) agrees well with the direct numerical integration (solid curve), Eq. (2.15), for times $t - T > T_2^*$. However, there is a disparity in the two cases for short times $t - T \simeq T_2^*$, since the assumption of infinite Doppler width σ in (3.37) results in a discontinuity at $t = T$ due to the first-order FID. We show below for the case of large pulse areas that a good approximation to (3.37) is the first term $(\alpha/r)^2 J_2(\alpha\chi T)$, which gives the same zero crossings as the infinite sum but differs in amplitude. The number of terms m needed to achieve a reasonable fit with direct numerical integration increases with pulse area and in Figs. 2 and 3 follows the sequence $m = 3, 3, 5, 8, 18$, and 40 as χT increases. Figure 4 is a blowup for the case $\chi T = 20\pi$ and allows the small-amplitude oscillations to be seen more clearly as $t \to 2T$. The envelope of the Bessel-

function sum (dashed curve) damps somewhat less rapidly than the numerical integration. We also notice slight differences in the zero crossings near $t=2T$. Such small differences, as shown in Fig. 4, are due to the finite Doppler width in the numerical integration. From an argument given below, ten periods of oscillation are expected here ($\chi T/2\pi=10$), but only nine are seen owing to the relative magnitude and location ($2T-t \approx 10^{-3}$ T) of the tenth oscillation.

Limiting cases: asymptotic form. For large arguments z, we may use the asymptotic expansion[20]

$$J_{2m}(z) \to (-1)^m (2/\pi z)^{1/2} \cos(z - \tfrac{1}{4}\pi), \tag{3.38}$$

and obtain a limiting result for the sum (3.37),

$$I(t) = -(2\pi)^{1/2} g(0) (\chi^{1/2}/t^{1/4}T)(2T-t)^{3/4} \times \cos\{\chi[t(2T-t)]^{1/2} - \tfrac{1}{4}\pi\}, \quad T<t<2T. \tag{3.39}$$

In Fig. 5, a computer plot of the asymptotic expression (3.39) (dashed curve) is overlayed on the numerical integration (2.15) (solid curve). The agreement is quite satisfactory except in the vicinity $t \to T$.

Note that (3.39) exhibits a number of important characteristics of oscillatory FID. First, the factor $(2T-t)^{3/4}$ reveals that the oscillation envelope decays approximately with a $\frac{3}{4}$ power law and reaches a zero-amplitude value precisely at $t=2T$. Second, the cosine argument contains an oscillation frequency that increases at $t \to 2T$. Third, since the phase $\chi[t(2T-t)]^{1/2}$ advances by χT in the interval $T<t<2T$, the number of oscillations is given by $\sim\chi T/2\pi$. Last, taking only the first term ($m=1$) in the sum (3.37) and using the asymptotic limit (3.38), we find

$$I(t) = -2(2\pi)^{1/2} g(0) (\chi^{1/2}/t^{5/4})(2T-t)^{3/4} \times \cos\{\chi[t(2T-t)]^{1/2} - \tfrac{1}{4}\pi\}, \quad T<t<2T. \tag{3.40}$$

Thus the asymptotic limit of the first term in the Bessel-function sum is the dominant term, as it approximates the asymptotic limit of the entire sum to within the factor $t/2T$. Nevertheless, the factor $t/2T$ is important as it scales the amplitude making (3.39) more precise than (3.40).

$t \to T$. In this limit, $\alpha \to 1$, $r \to 1$, and the sum (3.37) reduces to

$$I(t \to T) = \pi g(0) \chi [1 - J_0(\chi T)], \tag{3.41}$$

which reproduces (3.12) and (3.20) since $w(0)=-1$ and $g(0)=N/\sqrt{\pi\sigma}$ for a Gaussian line shape.

$t \to 2T$. In this case, $\alpha \to 0$, $r \to 2$, and (3.37) becomes

$$I(t \to 2T) = \tfrac{1}{4}\pi g(0) \chi^3 (2T-t)^2, \tag{3.42}$$

and reproduces (3.13) and (3.21).

IV. CONCLUSION

This paper predicts an unusual oscillatory FID effect which follows coherent preparation by a resonant square-wave electromagnetic pulse. Both numerical and analytic results are obtained from solutions of the Bloch equations. Oscillations are expected when the atomic sample is inhomogeneously broadened ($T_2^* \ll T_2$) and the pulse area satisfies the condition $\chi T \geq 2\pi$. In NMR, the free-induction-decay measurements of Bloom confirm such oscillations (incorrectly called "edge echoes") where $\chi T = 4\pi$ while in the infrared, the observations of Brewer and Shoemaker support our prediction for the case $\chi T = 1.5\pi$. More recently, Szabo and Kroll[23] have found interferences in optical FID which they attribute to the edge echo. However, for their conditions ($\chi T = 4\pi$, $T_2 = 2$ μsec, $T = 7$ μsec, and $\sigma = 1.6\pi$ nsec^{-1}), the envelope function decays far too rapidly (~30 nsec) to resemble even qualitatively the $\chi T = 4\pi$ curve of Fig. 3. Nevertheless, future optical or NMR experiments might illustrate this phenomenon even more decisively using larger pulse areas. Finally, two-pulse echoes having large pulse areas should display oscillations also. However, our numerical calculations show, in agreement with Mims,[24] that the echo shape function is a complicated pattern and does not display the uniform oscillations predicted here for pulsed free-induction decay.

ACKNOWLEDGMENT

This work is supported in part by the U. S. Office of Naval Research. N. C. W. acknowledges support of a Hertz Foundation Graduate Fellowship.

APPENDIX

We continue the derivation of (3.34) beginning with (3.33),

$$I_P(T) = \frac{2\pi g(0)}{t} \int_0^z \sinh\left(\frac{z^2 - z'^2}{2\chi t}\right) z' J_0(z') dz'. \tag{A1}$$

Note that

$$\sinh\left(\frac{z^2 - z'^2}{2\chi t}\right) = \sum_{m=0}^{\infty} \left(\frac{z^2 - z'^2}{2\chi t}\right)^{2m+1} \frac{1}{(2m+1)!} = \sum_{m=0}^{\infty} \sum_{j=0}^{2m+1} \frac{(z^2)^{2m+1-j}(-z'^2)^j C_j^{2m+1}}{(2\chi t)^{2m+1}(2m+1)!}, \tag{A2}$$

where the second step involves the binomial expansion of $(z^2 - z'^2)^{2m+1}$ and $C_j^{2m+1} \equiv \binom{2m+1}{j}$. Then (A1) is given by

$$I_P(T) = 2\pi \frac{g(0)}{t} \sum_{m=0}^{\infty} \sum_{j=0}^{2m+1} \frac{(-1)^j z^{2(2m+1-j)}}{(2\chi t)^{2m+1}(2m+1-j)!j!} \times \int_0^z z'^{(2j+1)} J_0(z')dz' . \quad \text{(A3)}$$

Integration by parts and the relation

$$\frac{d}{dz}[z^n J_n(z)] = z^n J_{n-1}(z) \quad \text{(A4)}$$

yield

$$\int_0^z z'^{2j+1} J_0(z')dz' = \sum_{l=0}^{j} (-1)^l \frac{j!2^l}{(j-l)!} z^{2j+1-l} J_{l+1}(z) . \quad \text{(A5)}$$

The inclusion of (A5) and (A3) results in a triple sum of Bessel functions

$$I_P(T) = 2\pi \frac{g(0)}{t} \times \sum_{m=0}^{\infty} \sum_{j=0}^{2m+1} \sum_{l=0}^{j} \frac{(-1)^{j+l} 2^l z^{(4m+3-l)} J_{l+1}(z)}{(2\chi t)^{2m+1}(2m+1-j)!(j-l)!} \quad \text{(A6)}$$

which can be rearranged to give

$$I_P(T) = 2\pi g(0)\chi \sum_{m=0}^{\infty} \left(\frac{z}{\chi t}\right)^{2m+2} \times \left(\sum_{j=0}^{2m+1} \sum_{l=0}^{j} \frac{(-1)^{j+l} (\frac{1}{2}z)^{2m+1-l} J_{l+1}(z)}{(2m+1-j)!(j-l)!} \right) . \quad \text{(A7)}$$

The limits on the double sum in brackets can be rewritten as

$$\sum_{j=0}^{2m+1} \sum_{l=0}^{j} \rightarrow \sum_{l=0}^{2m+1} \sum_{j=l}^{2m+1} , \quad \text{(A8)}$$

the arguments remaining unaltered. The double sum in brackets then takes the form

$$\sum_{l=0}^{2m+1} (\tfrac{1}{2}z)^{2m+1-l} J_{l+1}(z) \sum_{j'=0}^{r'} \frac{(-1)^{j'+2l}}{(r'-j')!j'!} = \sum_{l=0}^{2m+1} \frac{(\frac{1}{2}z)^{2m+1-l} J_{l+1}(z)}{(2m+1-l)!} \sum_{j'=0}^{r'} (-1)^{j'} C_{j'}^{r'} , \quad \text{(A9)}$$

where

$$r' \equiv 2m+1-l, \quad j' \equiv j-l ,$$

$$\sum_{j'=0}^{r'} (-1)^{j'} C_{j'}^{r'} = \delta_{r',0} = \delta_{2m+1,l} .$$

In this way the double sum (A9) becomes a single term of $J_{2m+1}(z)$, and (A7) reduces to the remarkably compact form

$$I_P(T) = 2\pi g(0)\chi \sum_{m=1}^{\infty} \left(\frac{z}{\chi t}\right)^{2m} J_{2m}(z) , \quad \text{(A10)}$$

which is the desired result (3.34).

---

*On leave from the Dept. of Physics, Univ. Essen, Gesamthochschule, Essen, W. Germay.

[1]R. G. Brewer and R. L. Shoemaker, Phys. Rev. A 6, 2001 (1972).

[2]K. L. Foster, S. Stenholm, and R. G. Brewer, Phys. Rev. A 10, 2318 (1974).

[3]R. G. Brewer and A. Z. Genack, Phys. Rev. Lett. 36, 959 (1976).

[4]A. Z. Genack, R. M. Macfarlane, and R. G. Brewer, Phys. Rev. Lett. 37, 1078 (1976).

[5]H. DeVries, P. DeBree, and D. A. Wiersma, Chem. Phys. Lett. 52, 399 (1977).

[6]A. Z. Genack and R. G. Brewer, Phys. Rev. A 17, 1463 (1978).

[7]R. G. DeVoe and R. G. Brewer, Phys. Rev. Lett. 40, 862 (1978); Phys. Rev. A 20, 2449 (1979); P. F. Liao, J. E. Bjorkholm, and J. P. Gordon, Phys. Rev. Lett. 39, 15 (1977).

[8]R. G. DeVoe, A. Szabo, S. C. Rand, and R. G. Brewer, Phys. Rev. Lett. 42, 1560 (1979).

[9]F. A. Hopf, R. F. Shea, and M. O. Scully, Phys. Rev. A 7, 2105 (1973).

[10]A. Abragam, *The Principles of Nuclear Magnetism* (Oxford University, New York, 1961); C. P. Slichter, *Principles of Magnetic Resonance* (Harper and Row, New York, 1963).

[11]S. Haroche in *High-Resolution Laser Spectroscopy*, edited by K. Shimoda (Springer, Berlin, 1977), p. 253.

[12]R. L. Shoemaker and R. G. Brewer, Phys. Rev. Lett. 28, 1430 (1972); R. G. Brewer and E. L. Hahn, Phys. Rev. A 11, 1641 (1975).

[13]A. L. Bloom, Phys. Rev. 98, 1105 (1955).

[14]M. Sargent, M. O. Scully, and W. E. Lamb, Jr., *Laser Physics* (Addison-Wesley, Reading, Mass., 1977).

[15]R. G. Brewer in *Frontiers in Laser Spectroscopy* (North-Holland, Amsterdam, 1977), Vol. 1, p. 341.

[16]A. Schenzle, N. C. Wong, and R. G. Brewer (unpublished).

[17]H. C. Torrey, Phys. Rev. 76, 1059 (1949).

[18]A. Schenzle and R. G. Brewer, Phys. Rev. A 14, 1756 (1976).

[19]H. Bateman, *Tables of Integral Transforms* (McGraw-Hill, New York, 1954), Vol. I, p. 248.

[20]*Handbook of Mathematical Functions*, edited by M. Abramowitz and I. A. Stegun (Dover, New York, 1972), p. 355.

[21]I. S. Gradshteyn and I. W. Ryzhik, *Table of Integrals, Series and Products* (Academic, New York, 1965), p. 472.

[22]G. F. Simmons, *Differential Equations* (McGraw-Hill, New York, 1972), p. 90.

[23]A. Szabo and M. Kroll, Opt. Lett. 2, 10 (1978).

[24]W. B. Mims, Phys. Rev. 141, 499 (1966).